Journal of Engineering and Applied Science Vol. 08, No. 02, pp. 115–124, December 2024

Journal of Engineering and Applied Science
Contents are available at www.jeas.ruet.ac.bd

Time of flight methods for thickness measurement of aluminium plane plate using the thermoelastic regime in laser UT

Md. Abdur Rahim[1,*], Yoshio Arai[2]

[1] *Department of Mechanical Engineering, Rajshahi University of Engineering & Technology, Bangladesh*
[2] *Graduate School of Science and Engineering, Saitama University, Japan*

ARTICLE INFORMATION

Received date: 30th Sep 2024
Revised date: 27th Dec 2024
Accepted date: 27th Dec 2024

Keywords

Laser ultrasonics
Time of flight
Thermoelastic regime
Non-destructive
Propagation velocity

ABSTRACT

Conventional LUT methods often struggle with significant noise in low-intensity waveforms, which compromises measurement accuracy. Instead of generation pulse, reflection pulses which are affected by low velocity waves after back reflection are normally used to calculate the time of flights. Accuracy obtained about 10%, 0.100, 0.050 mm etc. This paper presents a combined numerical/experimental effort to accurately measure thickness in case of plane aluminium plate experimentally using Laser Ultrasonic Technique (LUT) and find suitable time of flight methods and investigate the wave propagation characteristics using simulations. Lower generation laser power is used therefore no visible ablation spot on the material surface which is highly expected, and the phenomena is referred to as thermoelastic regime. Comparatively higher amplitudes of waveforms are produced which is easy for obtaining precise peaks with curve fitting methods which includes also the generation pulse. Time dependent multiple waveforms data are averaged to get waveform with less noise and stable pulse from which better method of time of flight is evaluated. Variation of time of flights occur which is revealed by simulation results. The inclusion of generation pulse for calculating the time of flight using -6dB method would be the better method for thermoelastic regime.

1. Introduction

Non-contact thickness measurement is essential in situations where direct access is difficult or environmental conditions are unfavorable. Precise thickness measurements are often required, and conventional contact methods, like micrometers, are limited to objects edge measurements and prone to alignment errors. Contact ultrasonic gauges struggle with irregular or inclined surfaces due to their flat measurement head [1]-[2]. Its working also effected by surrounding conditions etc. In such cases, a non-contact method for thickness measurement is essential [3]-[4]. Non-contact measurement is highly suitable with better accuracy and all environment conditions.
In this study, Laser Ultrasonic Testing (LUT) offers a non-contact and non-destructive method for material characterization, including thickness measurement, by utilizing the thermoelastic regime. In our previous studies reasonable accuracy is obtained using thermoelastic regime [5]-[6] and ablation regime [7]. Thermoelastic regime of LUT has been studied experimentally [8]-[9] and using simulation [10]-[13]. In those previous studies waveforms with sinusoidal

* Corresponding authors: Department of Mechanical Engineering, Rajshahi University of Engineering & Technology (RUET), Bangladesh
E-mail addresses: rahimruet05@gmail.com (Md. Abdur Rahim)

shapes and having significant amount of noise. The presence of noise necessitates advanced processing techniques, such as waveform averaging or filtering, to enhance precision, particularly in the thermoelastic regime using Laser Ultrasonic Testing (LUT). Reducing noise and obtaining clearer waveforms are critical for improving the reliability of the measurement data. In the current study, different methods have been used to get better one with reasonable accuracy.

Much research has been conducted experiments and simulations on LUT thickness measurements. Pure sinusoidal waveform is not observed. For that reason, different filtering techniques etc. are applied to the waveforms for getting accuracy [14]-[18].

Since measuring the thickness of plane plates, the method should be clear. Several researchers have applied different procedures to process data as well as to modify the waveforms etc. to find representative time. Those previous studies show waveforms with low intensity and not sinusoidal or sharp pulse [19]. Accuracy is also affected by different parameters such as ablation, temperature as well as thickness variation. If we can use the thermoelastic regime to predict the thickness it will be a advanced technique to measure thickness remotely and non-destructively. There will be no ablation spot due to generation laser hitting.

To the best of the author's knowledge, no research has yet been reported on the use of time-of-flight methods to enhance the accuracy of thickness measurements by averaging multiple waveforms in the thermoelastic regime using Laser Ultrasonic Testing (LUT). The present study describes a time of flight measurement technique of aluminium alloy specimens by using LUT at thermoelastic regime and finding better representative times for the time of flight methods using experimental and simulation approach.

In this study we present new approaches to enhancing the accuracy of non-contact, non-destructive thickness measurements of aluminum alloy specimens using LUT in the thermoelastic regime. Our methodology focuses on refining time-of-flight measurement techniques by averaging multiple waveforms to mitigate noise and improve precision. Inclusion of the generation pulse for time of flight calculation offers a effective method. We employ both experimental and simulation approaches to identify optimal representative times for time of flight calculations, aiming to establish a reliable and innovative technique for remote thickness measurement without the drawbacks associated with ablation. This study contributes to the advancement of LUT applications in material characterization, offering potential improvements in measurement reliability across various environmental conditions.

2. Materials and methods

Plain plate specimens

The plain plate specimen is shown in **Figure 1.** The thickness of specimen is 2.709 mm. Measurement locations are near the middle of the specimen. Surface finishing process such as milling and polishing are done to get super surface finish. Material of Al 6061T6 [20] is used as the specimen for thickness measurement. The selection of aluminium, specifically Al6061T6, as the material for LUT thickness measurement is well-justified due to its widespread industrial applications, excellent mechanical properties, and good thermoelastic response under laser excitation. Aluminium has relatively high thermal conductivity, moderate density, and isotropic behaviour make it an ideal candidate for exploring the capabilities and limitations of LUT techniques.

Materials like steel or titanium may require higher laser power for equivalent ultrasonic generation due to their higher melting points and lower thermal diffusivity, increasing the risk of ablation. Polymers and ceramics often have lower thermal conductivities, which could lead to localized heating and uneven wave generation.

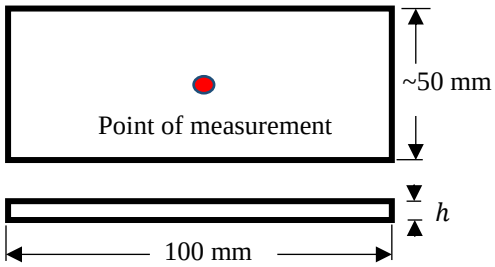

Figure 1. Points of measurement on same material divided into two.

Compression test and Mechanical properties

The specimen with length, width and height of 18.022 mm, 10.019 mm, 10.019 mm respectively are used in the compression test. The material constant found from the compression test and density test of the specimen is shown in **Table 1**.

Table 1. Material Properties by compression test.

Parameters	Value
Yong Modulus (MPa)	70700
Poisson's ratio	0.35
Density (Kg/m^3)	2700

The material properties listed above are used to compare with the one used for calibration of simulation results.

Method of thickness measurement using LUT

The experimental set-up of the LUT is shown in **Figure 2**. The AC voltage is recorded from the oscilloscope, which is generated in the receiver unit. This occurs as the receiver sensor detects the surface movement caused by the generation laser, and the signal is then processed.

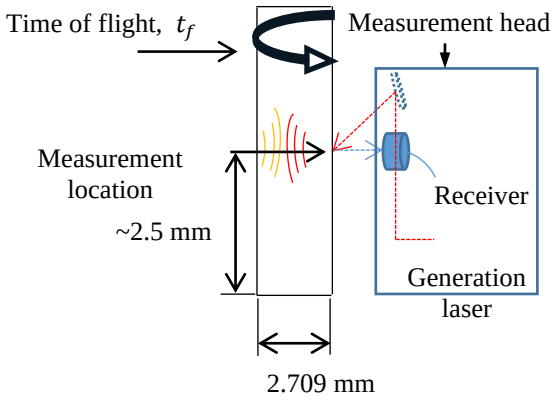

Figure 2. Thickness measurement using LUT.

When wave generated at the front surface and after reflection at the back surface, it comes to the front surface the time required for such single step is called the time of flight t_f or round trip time. The time of flight t_f using thickness is calculated using equation 3 as follows.

$$t_f = \frac{h \times 2}{\bar{V}} \quad (1)$$

where, h is the thickness of the is the thickness of the plane plate specimen and $\bar{V}$ is the theoretical velocity (~6392 m/s) of a laser-generated longitudinal wave in A6061-T6. The resolution of time measurement is 1 ns.

When determining the thickness measurement, a longitudinal wave is taken into account. This is because longitudinal waves propagate more quickly than shear waves [21]. In the thermoelastic regime strong edge generated shear wave produced which overlaps the longitudinal wave hence effect round trip time which is needed to investigate. The primary and admirable aspect of this research is that the producing and receiving lasers operate simultaneously on the same side and at the same spot. In order to improve the accuracy of thickness assessment using this method, wave overlapping can be reduced.

Table 2 lists the parameters for the lasers used in the generation and reception. The primary and admirable aspect of this research is that the producing and receiving lasers operate simultaneously on the same side and at the same spot. In order to improve the accuracy of thickness assessment using this method, wave overlapping can be reduced.

Table 2. Specifications of the Laser UT device.

Generation laser	Receiving laser
Wavelength: Q-switched Nd: YAG at 1064 nm	Wavelength: Single-frequency fiber laser at 1550 nm
Pulse width: 10 ns	Continuous wave
Pulse energy~ 40 mJ.	Power: 2 W
Focus diameter: ~2 mm	Focus diameter: ~0.2 mm

We used only around 19.2 mJ laser power and in this condition, LUT is harmless to the material.

Experiment using different power of the LUT

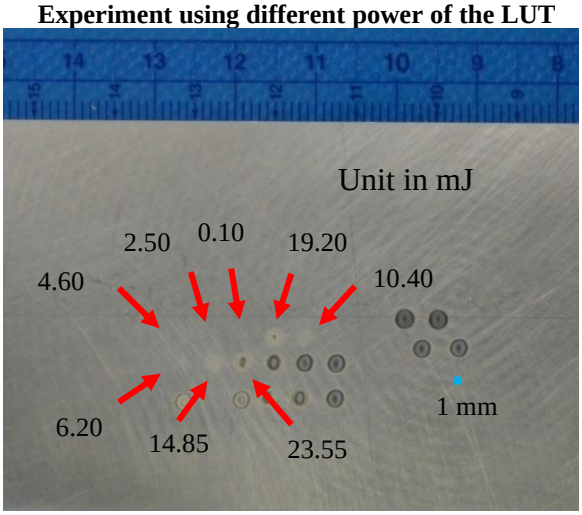

Figure 3. Spots of thermoelastic regime.

The generation laser spots for different laser energy is shown in **Figure 3.** We can see at low laser power ablation spot is not visible. It is very important if we can measure thickness with LUT without any scratches on metal surface. It is defined as thermoelastic regime. The feasibility of thickness measurement using thermoelastic regime is needed to investigate.

Methods and representative points for time of flight

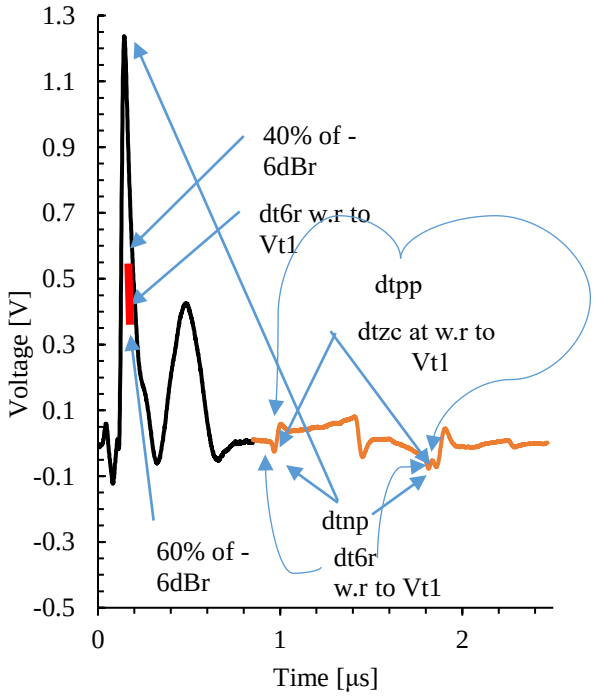

Figure 4. Illustration of representing time for time of flight calculation.

Table 3. Methods and corresponding representative points for time of flight calculations.

Methods	Name	Representative points	Time of flight
1	6rg1	-6dB at rising pulse (Generation and 1st reflection)	dt6rg1
2	npg1	Positive to negative peaks (Generation and 1st reflection)	dtnpg1
3	6r12	-6dB at rising pulse (1st and 2nd reflections)	dt6r12
4	np12	Negative peaks (1st and 2nd reflections)	dtnp12
5	zc12	Average-cross (Average value of positive and negative peaks)	dtzc12
6	pp12	Positive peaks (1st and 2nd reflections)	dtpp12

The calculation methods of time of flight with corresponding representative time are shown in **Figure 4** and **Table 3**. For finding the peak of curve the negative part of the generation pulse and both the negative and positive part of the reflection pulses polynomial curve fitting of third order are used. The bound of the curve is about half of the bare maximum voltage of the generation pulse for both rising and falling side of the negative generation and both negative and positive reflection pulses. The equation of the curve fitting is given below-

$$V(t) = at^3 + bt^2 + ct + d \quad (2)$$

Where, t is time and a, b, c, d are constants.

For finding the maximum value i.e. peak point it is needed to differentiate equation and the results should be zero and the corresponding time value is shown in the in equation 5.

$$\frac{dV}{dt} = 0$$
$$t = \frac{-2b \pm \sqrt{4b^2 - 12ac}}{6a} \quad (3)$$

For finding the time of flight using zero cross method, linear fitting is used. For calculating the time of flight using -6dB method, the rising side (left side) of both generation pulse and the reflection pulses are used. The line bounded by 40% and 60% of the maximum voltage point (peak point) of the polynomial curve fitting is used. The half of the maximum voltage of the fitting curve is used as the voltage $Vt1$ as shown below to calculate the representative time $t1$ for the -6dB method. In case of zero-cross method, both $Vt1$ and line range (40% and 60%) is taken as the average values of the maximum voltage of the fitting curve of the negative and positive part of the reflection pulses.

$$\mathrm{Vt1} = ct1 + d$$
$$t1 = (Vt1 - d)/c \quad (4)$$

Simulation method for the plane plate specimens

Heat-flux are used as load in the simulations which is defined as the thermoelastic regime simulations to calibrate the experiments. Modelling, boundary conditions, calibration procedure etc. are discussed in this section.

Modeling of the simulation. The simulation model with necessary dimensions is shown in **Figure 5**.

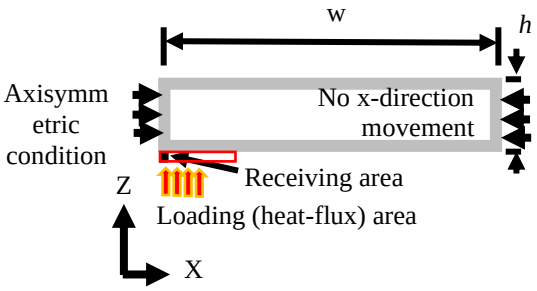

Figure 5. Simulation model with dimensions and boundary conditions.

Due to limitations of the number of elements in the 3D simulation, an axisymmetric model of the plane plate is used. To reduce calculation time the width (w) of the simulation model is taken 9 mm and the thickness (h) is 2.709 mm which is exactly same as the experiment. The loading area is taken as 1 mm wide as radius which is measured from ablation spot radius in the LUT experiments. The receiving area is taken as 0.1 mm wide as radius.

Meshing for the model. Fine mesh of size 3 µm are used to capture the wavefront properly and within short interval of time up to nano second order. Illustration of mesh distribution is shown in **Figure 6** and others meshing parameters are shown in **Table 4**. Abaqus explicit solver is used for calculation.

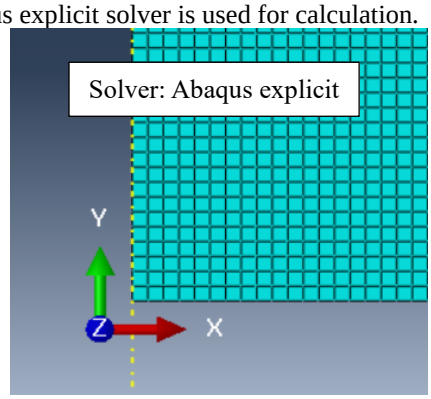

Figure 6: Fine meshing.

Table 4. Meshing of the simulation model.

Element type	CAX4R
Maximum number of elements	7524699
Maximum number of nodes	7533936
Element size	3 µm

Calibration of the material constant in simulation. The flow chart for the calibration of material constant is shown in **Figure 7.**

The contact gauge is used to initially measure the thickness three times and are averaged. Time of flights then calculated using averaged waveforms data obtained from LUT experiments. And finally, FEM simulation is constructed to calibrate the experimental time of flight. By keeping one material property constant others are varied and width of the Gaussian amplitude curve are varied to get similar time of fight between generation to 1st reflection pulse with the experiment. After conducting numerous simulations time of flight is matched with the experimental time of flight.

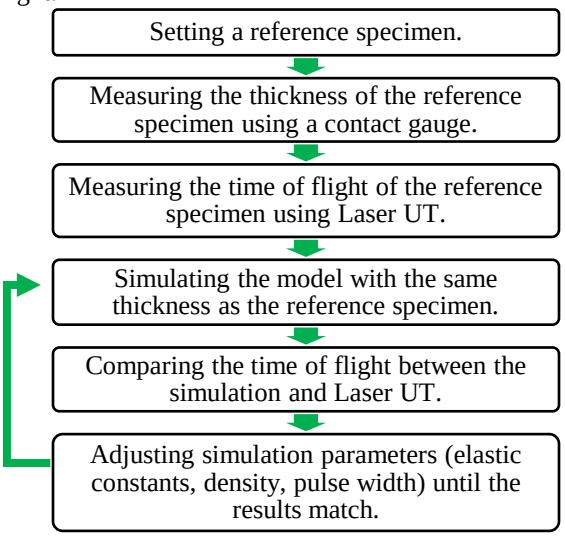

Figure 7. Flow chart for calibration of material constant.

Amplitude chart for thermoelastic simulations. For thermoelastic regime (temperature) simulations Gaussian function is used as below

$$\boldsymbol{p(t) = e^{-\frac{(t-t_0)^2}{k}}} \quad (5)$$

Where, t_0, k are the controlling parameters for pulse length (time) and pulse width respectively of the amplitude curve for ablation simulation. The values are $1.85 \times 10^{-7} s$ and $5 \times 10^{-16}\, s^2$ respectively. The equation 5 is used to get amplitude curve for thermoelastic simulations.

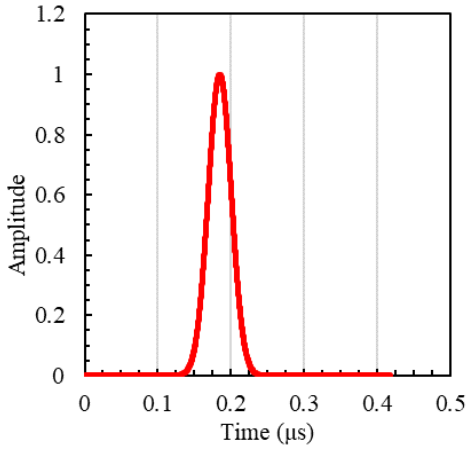

Figure 8. Input pulse shape for thermoelastic simulations.

The amplitude curve is constructed to match with the shape as well as representative points of time of flight with the experimental waveforms. The representative points of npg1 of the experiment is used as reference for representative points of amplitude curve as shown in **Figure 8.**

Temperature dependency of the material properties in thermoelastic simulation. Several researchers [22]-[25] have done thermoelastic simulation with temperature dependent material properties. The summarized relations are shown in the following equations -

$$\rho = -0.22T + 2769 \rightarrow 300 \leq T \leq T_m \quad (6)$$

$$K(T) = \begin{cases} 292.6 \rightarrow T < 200 \\ 249.45 - 0.085T \rightarrow 200 < T < 730 \\ 198.47 - 0.0148T \rightarrow 730 < T_m \end{cases} \quad (7)$$

$$C_p(T) = \begin{cases} 3.971T \rightarrow T < 200 \\ 780.27 + 0.488T \rightarrow 200 \leq T \leq T_m \end{cases} \quad (8)$$

Where ρ, K and C_p are the density, thermal conductivity and specific heat capacity used as the material properties. T is the temperature in Kelvin. The others material properties are used as same as used in compression test and calibrated parameters.

Method of wave propagation velocity calculation in thermoelastic simulation. Wave propagation velocities are calculated for thermoelastic simulation for comparison. Wave propagation velocity is calculated dividing the average value of representative points difference (Z coordinate) by the time difference among there successive pulse as shown in **Figure 9.** Two representative points pp_z and $6r_z$ are used.

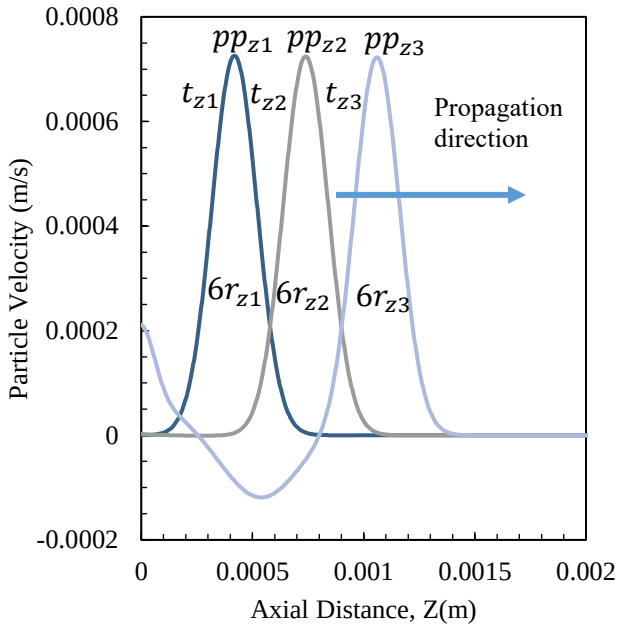

Figure 9. Propagation velocity calculation from successive pulses along Z-axis.

$$\text{1st Average, } pp_{avg1} = \frac{pp_{z1} + pp_{z2}}{2}$$

$$\text{2nd Average, } pp_{avg2} = \frac{pp_{z2} + pp_{z3}}{2}$$

$$\text{1st Average, } t_{avg1} = \frac{t_{z1} + t_{z2}}{2}$$

$$\text{2nd Average, } t_{avg2} = \frac{t_{z2} + t_{z3}}{2}$$

$$Thus, propagation\ velocity\ using\ \text{1st and 2nd positive peaks} = \text{ABS}\left(\frac{\text{2nd Average, } pp_{avg2} - \text{1st Average, } pp_{avg1}}{\text{2nd Average, } t_{avg2} - \text{1st Average, } t_{avg1}}\right) \quad (9)$$

In a similar way, propagation velocity are calculated using successive -6dBr rising points and pp representative points.

3. Results and discussion

Time dependence of the waveforms

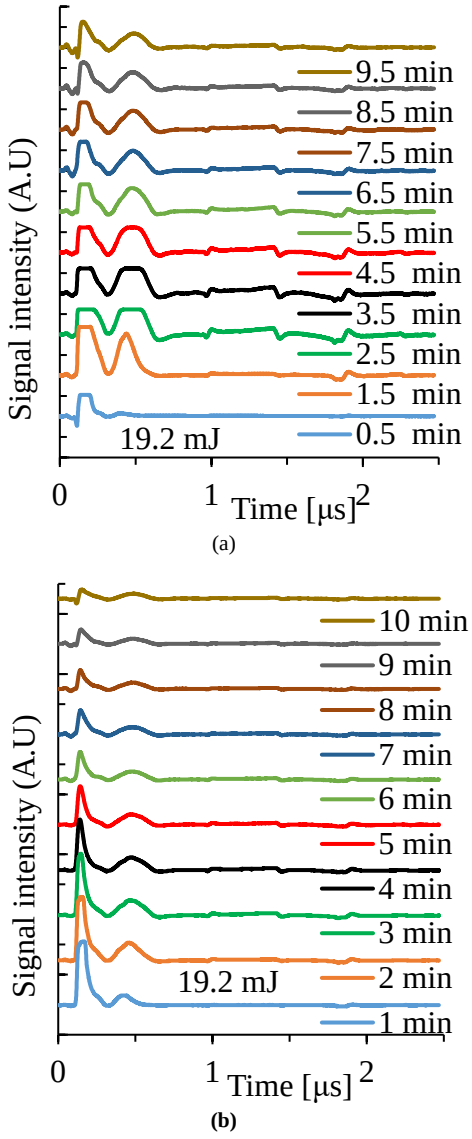

Figure 10. Waveforms for thermoelastic (a) for reflection pulses and (b) for generation pulses.

Time dependent (1 minute interval) waveforms for reflection pulses (19.2 mJ) are shown for thermo-elastic regime in (a), (b) respectively in **Figure 10**. Initially, no reflection pulses until around 2 min. After that, regular reflection pulses with initially negative and then positive peaks are produced.

At first vertical scale of the Oscilloscope is kept small (~100 mV) to get better amplitude of the reflection pulses (1st and 2nd reflection). In this case, generation pulse is saturated (no sharp peak) as shown in (a). As high voltage is produced in case of generation pulse; to get sharp peak, the vertical scale of the Oscilloscope is kept high around 1 V and the resultant pulses are shown in b. The amplitude of the generation pulse gradually decreases over the time as shown in (b). But reflection pulses initially increase and then gradually decrease.

Therefore, for calculation of time flights 1st five waveforms (until 5 minutes) are not considered. That is, Average values of the stable waveforms are considered. In reflection cases 5.5 to 9.5 min waveforms data are averaged whereas for generation pulse 6 to 10 min waveforms data are averaged for making time dependent similarity.

Energy dependence of the waveforms

For different laser energies, using same vertical scale increment (0.5 V), the waveforms for reflection pulses are shown in **Figure 11** (a) and using same vertical scale increment (1 V), the waveforms for generation pulses are shown **Figure 11** (b). As a definition, waveforms for 23.55 mJ laser energy is the transition waveform and the waveforms for the 19.2 mJ to minimum laser energy 14.85 mJ are called the thermo-elastic regime. Signal intensity increases gradually in thermoelastic regime.

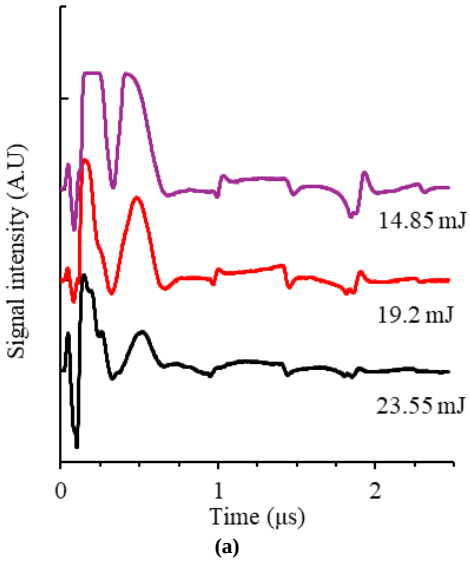

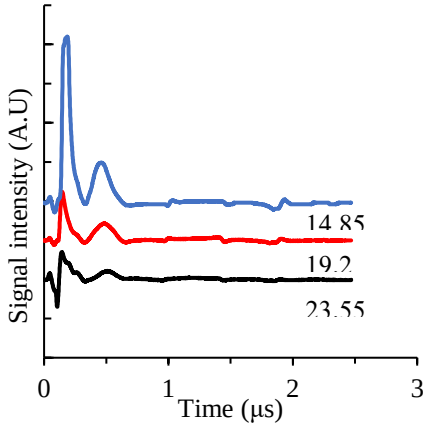

(b)

Figure 11. Waveforms of average data for thermoelastic (a) for reflection and (b) for generation.

Generation and reflection waveforms of average data

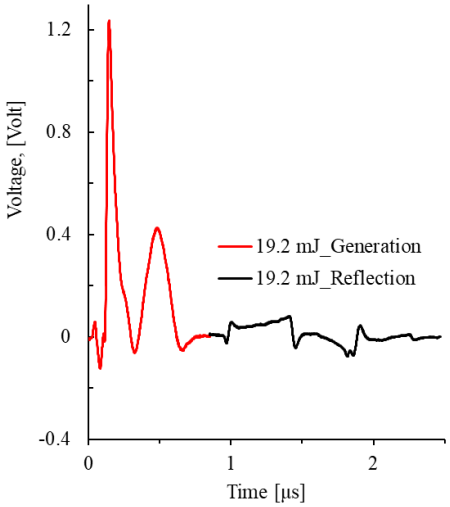

Figure 12. Waveforms for generation and reflection pulses in thermoelastic-regime.

Waveforms for thermoelastic regimes are shown in **Figure 12.** As already have mentioned before, waveform for the generation pulse and reflection pulses are at different vertical scale of the oscilloscope to get sharp peaks (not saturated).

The second reflection signal intensity is higher than the 1st reflection signal intensity. The are two downward peaks in case of the second reflection. The 1st peak is taken as representative point for time of flight calculations.

Relation between time of flights and laser power

Variations of time of flights corresponding to the different laser energies in thermoelastic regime are shown in **Figure 13**. Reduction in the time of flight occurs when laser energy is reduced from ~23.55 mJ to ~14.85 mJ except dtnp12 which increases. The time of flight dt6r12 shows the less variation hence better method compared to other time of flight of calculation.

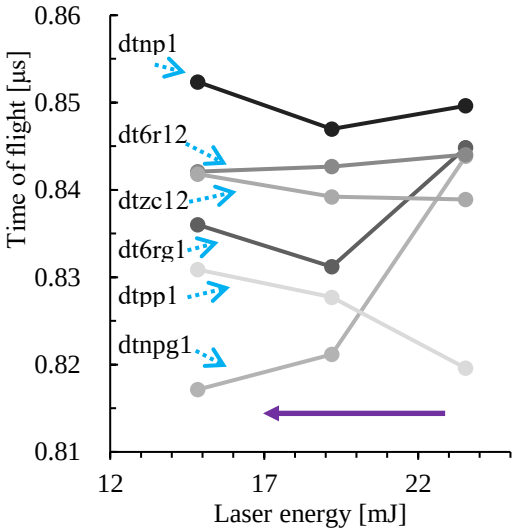

Figure 13. Laser energy vs time of flight for different representative time.

The deviation occurred mainly in case of thermo-elastic regime with lower laser energy. In thermo-elastic regime, the generation pulses are not so sharp at peak points and apparent time of flight between the generation and first reflection (dtnpg1, and dt6rg1) are shorter than the time of flights between1st to 2nd reflections for other methods.

Simulation results of plane plate with thermoelastic regime

Comparison between experiment (red curve) and simulation waveforms (black curves) for thermoelastic regime are shown in **Figure 14**. Difference in time between generation negative peak to the 1st reflection negative peak (npg1) of the experiment is taken as reference. We can see that all the pulse shapes between experiment and simulation are similar. The pulse width in case of experiment is slightly larger than that of the simulation. The reason lying behind this is that, the saturation occurs i.e. edge of the generation signal mixed with next signal.

We can see that the value of the npg1 in thermoelastic simulation is similar to the experiment as shown in **Table 5.** Other values are gradually increases in both simulation and experiments although some variations occur in case of 6r12, pp12 and zc12.

-6dB method is a widely utilized technique in ultrasonic testing, including laser ultrasonic testing for determining the time of flight of ultrasonic waves. Using this method, the onset of a reflection or pulse is accurately pinpointed. Therefore, variation of time of flight using this method is less specially when using generation pulse to 1st reflection pulse which has been mainly focused on this study.

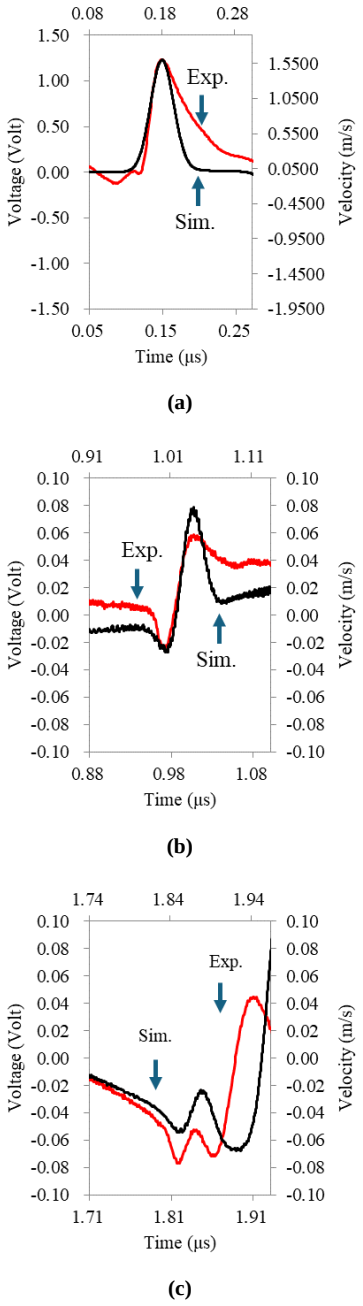

Figure 14. Comparison between experiment and simulation waveforms (a) generation pulses (b) 1st reflection pulses (c) 2nd reflection pulses.

Table 5. Comparison between experimental and Simulation time of flight.

Time of Flights	Laser Energy 19.2 mJ (Experiment)	Thermoelastic Simulation
npg1 (µs)	0.8212	0.8242
6rg1 (µs)	0.8312	0.8248
np12 (µs)	0.8470	0.8459
6r12 (µs)	0.8427	0.8031
pp12 (µs)	0.8277	0.8406
zc12 (µs)	0.8392	0.8560

Repeatability of the experiments

Laser power depended variability has been shown in **Figure 15**. Two laser energy levels of 19.2, 14.85 mJ have been used in the thermoelastic regime.

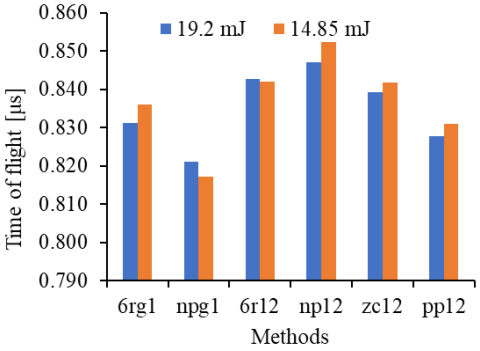

Figure 15. Power dependent repeatability of time of flights.

We can see that, little variation of the time of flights occurred when we use 19.2 mJ and 14.85 mJ. In this case also -6dB method shows the less variation of time of flight.

Comparative analysis

Several related research has been conducted on LUT thickness measurement methods. Comparison with recent work [5]-[6] is listed at **Table 6**.

Table 6. Comparison with literature.

Items	Literature	Current study
Methods	Generation and receiving points different	Generation and receiving points same
Accuracy	0.100 mm [5] 0.05 mm [6]	~ 2 µm
Velocity difference	70 m/s [5] 32 m/s [6]	~ 5 m/s
Specimen type	Only plane plate	Not limited to plane plate

In the current study column of **Table 6**, The accuracy is determined by subtracting the product of half the time of flight and the theoretical velocity from the original thickness of the plate. Velocity is obtained by dividing the original thickness by the time of flight. In those two cases we have used -6dB method for reflection pulses. Therefore, the -6dB method provides more accurate time-of-flight calculations in the thermoelastic regime. Other methods also show greater accuracy compared to the literature.

Reasons of variation of time of flights for thermoelastic regime

In the thermoelastic regime experiments we can see that, wave propagates in case of thermoelastic regime varied. The phenomena are discussed using simulation results here. The particle velocity along center (Z-axis)

for a specific time (increment or step in simulation) as shown in **Figure 16**. We can see that, significant amount of vibration is produced as strong edge generated wave is produced and dominates longitudinal wave as shown in contour plots of **Figure 18**.We can see that the wave propagation velocities are in case of thermoelastic regime simulation are varied in case of different method of the time of flights as shown in **Figure 17.** Some vibrations exist in which the calculation method has some effects. Initially, the average velocities (the middle positions of the sinusoidal wave) are same in case of both peak to peak and -6dB method for rising pulses. But later the wave propagation velocity is increased before reaching to the back surface. The pulse shape does not remain sinusoidal therefore getting peak to peak representative time using curve fitting method is difficult and we have used -6dBr method.

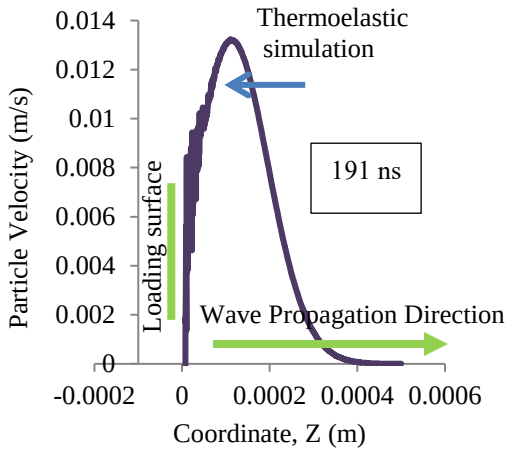

Figure 16. Particle wave velocity for different coordinates for thermoelastic and external load simulation.

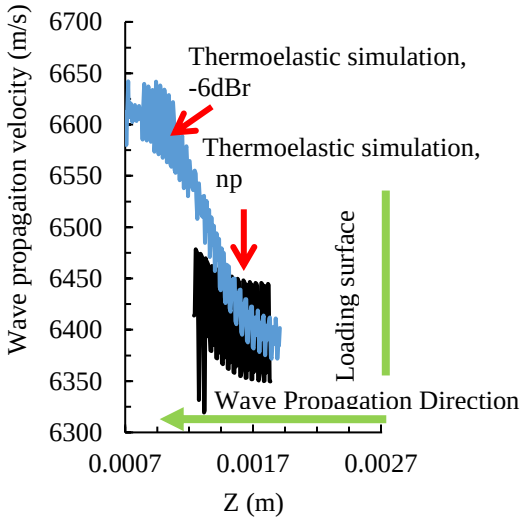

Figure 17. Wave propagation velocity for different coordinates for thermoelastic simulation.

The propagation characteristics for longitudinal and transverse waves for thermoelastic regime simulation are shown in **Figure 18** using contour plots. In case of both type of wave propagation, the wave propagation start from the edge of the loading surface. That means that oblique wave (edge generated shear wave) proceeds with higher velocity is in case of thermoelastic regime. Compressional wave in case of the transverse wave proceeds faster (as the location of the minimum value is higher) in case of thermoelastic simulation in **Figure 18**.

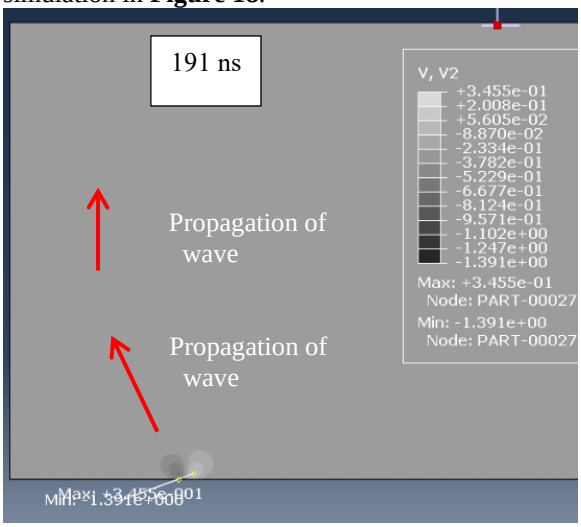

(a)

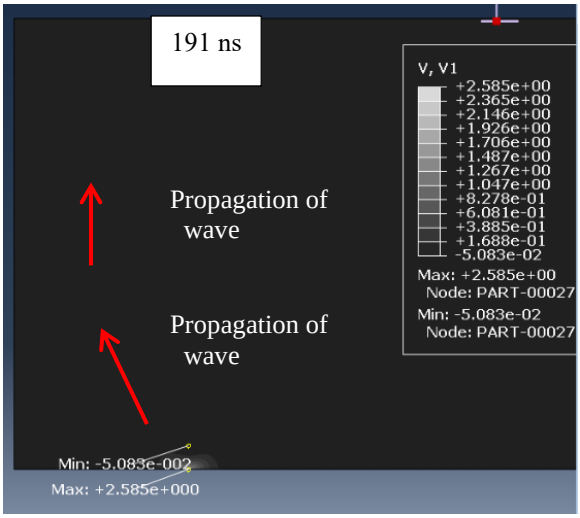

(b)

Figure 18. Longitudinal (a) and transverse (b) wave propagation at 191 ns in Thermoelastic regime.

Using the laser ultrasonic method, we cannot see the wave propagation characteristics that affect the time of flight. Using FE simulation we can investigate wave propagation velocities, direction etc. Therefore, causes of variation of time of flight in practical applications can be verified.

Due to the limitation of number of nodes (for fine meshing) for 3D model dimensionally same with the experiment, axisymmetric model is used. There are

some limitations of axisymmetric model like boundary conditions are simplified, distribution of laser generation amplitude curve is taken as Gaussian etc., which do not replicate real-world experimental conditions. To mitigate these limitations calibrations procedure has been adopted. Although there are some variations in the generation pulse width between experiment and simulation, pulse shape as well as peak point positions remain similar.

4. Conclusion

The proposed ultrasonic method using average waveforms gives reasonable values of time of flight in thermoelastic regime. The time of flights of -6dB at rising pulse between generation to 1st reflection and between the reflection pulses are the better methods for calculating the time of flight with more stability in thermoelastic regime. Strong edge generated shear wave generated with velocity higher than longitudinal wave in the thermoelastic regime. Therefore, wave propagation velocity is higher in case of -6dB method when calculated from the particle wave velocity waveforms from simulation results. The findings offer advancements in non-contact, non-destructive testing, with potential applications across various industries that rely on precise material characterization. The methods can be used to materials other than aluminium even for multilayer thickness measurement, modern composite materials etc.

Acknowledgements

I would like to acknowledge the financial assistance provided by the Ministry of Education, Culture, Sports, Science, and Technology of Japan Government in the form of MEXT scholarship. This study is supported by Rajshahi University of Engineering and Technology (RUET) and Strength of Material Laboratory of Saitama University and Asahi Seisakusho Co. Ltd., Japan.

References

[1] M. A. Rahim, Y. Arai, and W. Araki, “Effects of thickness variation due to presence of roller wake on the thickness measurement using laser ultrasonic technique,” The International Journal of Advanced Manufacturing Technology, vol. 132, no. 1–2, pp. 339–348, May 2024.

[2] J.P. Monchalin, C.Neron, J.F.Bussiere, “Laser-ultrasonics: from the laboratory to the shop floor,” Adv. Perform. Mater. vol.5, pp. 7-23, January 1998.

[3] Q. Vo, Y. Duan, X. Zhang, and F. Fang, "Non-contact method of thickness measurement for a transparent plate using a laser auto-focus scanning probe," Appl. Opt. 58, 9524-9531 (2019).

[4] P. Liu, A. W. Nazirah, and H. Sohn, “Numerical simulation of damage detection using laser-generated ultrasound,” Ultrasonics, vol. 69, pp. 248–258, Jul. 2016.

[5] N. T. Dung and Y. Arai, “Laser Ultrasonic Technique for Simultaneous Measurement of Thickness, Slope, and Wave Velocities for Slope Plate in the Thermoelastic Regime,” Adv. Sci. Technol. Res. J., vol. 18, no. 5, pp. 217–233, 2024.

[6] N. T. Dung and Y. Arai, “Simultaneous measurement of thickness and ultrasonic wave velocity using a combination of laser-generated multiple wave modes in the thermoelastic regime,” Nondestruct. Test. Eval., pp. 1–27, Jun. 2024.

[7] M. A. Rahim, Y. Arai, and W. Araki, “Difference in Thickness Measurement by Laser Ultrasonic Technique Using Time of Flight Methods,” SSRN Electron. J., no. December, pp. 1–6, 2024.

[8] J. Kim and K. Y. Jhang, “Non-contact measurement of elastic modulus by using laser ultrasound,” Int. J. Precis. Eng. Manuf., vol. 16, no. 5, pp. 905–909, 2015.

[9] S. N. Hopko and I. C. Ume, “Laser ultrasonics: Simultaneous generation by means of thermoelastic expansion and material ablation,” J. Nondestruct. Eval., vol. 18, no. 3, pp. 91–98, 1999.

[10] X. L. Tu, J. Zhang, A. M. Gambaruto, and P. D. Wilcox, “Finite element modelling strategy for determining directivity of thermoelastically generated laser ultrasound,” Ultrasonics, vol. 138, p. 107252, March 2024.

[11] J. C. Cheng, S. Y. Zhang, and L. Wu, “Excitations of thermoelastic waves in plates by a pulsed laser,” Appl. Phys. A Mater. Sci. Process., vol. 61, no. 3, pp. 311–319, 1995.

[12] M. V. Shugaev and L. V. Zhigilei, “Thermoelastic modeling of laser-induced generation of strong surface acoustic waves,” J. Appl. Phys., vol. 130, no. 18, 2021.

[13] J. Wang, Z. Shen, B. Xu, X. Ni, J. Guan, and J. Lu, “Simulation on thermoelastic stress field and laser ultrasound waveform in non-metallic materials by using FEM,” Appl. Phys. A Mater. Sci. Process., vol. 84, no. 3, pp. 301–307, 2006.

[14] J. Qiu, Z. Li, C. Pei, and G. Luo, “Simulation of Layer Thickness Measurement in Thin Multi-Layered Material by Variable-Focus Laser Ultrasonic Testing,” Sensors, vol. 23, no. 2, p. 694, Jan. 2023.

[15] M. Malmström et al., “Laser-Ultrasound-Based Grain Size Gauge for the Hot Strip Mill,” Appl. Sci., vol. 12, no. 19, 2022.

[16] W. Gong, X. Wang, Z. Yang, Z. Zhai, W. Feng, and D. Liu, “Ultrasonic Thickness Measurement Method and System Implementation Based on Sampling Reconstruction and Phase Feature Extraction,” Sensors, vol. 23, no. 22, p. 9072, Nov. 2023.

[17] C. Humer, S. Höll, C. Kralovec, and M. Schagerl, “Scattered Ultrasonic Guided Waves Characterized by Wave Damage Interaction Coefficients: Numerical and Experimental Investigations,” Sensors, vol. 22, no. 17, p. 6403, Aug. 2022.

[18] P. Siafarika, N. K. Nasikas, and A. G. Kalampounias, “How Ultrasonic Pulse-Echo Techniques and Numerical Simulations Can Work Together in the Evaluation of the Elastic Properties of Glasses,” Appl. Sci., vol. 13, no. 14, 2023.

[19] N. Smailov et al., “Numerical Simulation and Measurement of Deformation Wave Parameters by Sensors of Various Types,” Sensors, vol. 23, no. 22, p. 9215, 2023.

[20] H. Bawa’neh, B. Lababneh, A. M. Malkawi, and A. Bozeya, “Investigation of Aluminum (Al 6061-T6)/Graphene/Bentonite Hybrid Nanocomposite Mechanical Properties with Finite Element Analysis Study,” Mater. Adv., 2025 (Accepted Manuscript).

[21] A. Cavuto, F. Sopranzetti, M. Martarelli, G. M. Revel, and M. Sciences, “Laser-Ultrasonics Wave Generation and Propagation FE Model in Metallic Materials Introduction : Laser-Ultrasonics,” vol. 2, no. 2, 2013.

[22] G. Chen, X. Gu, and J. Bi, “Numerical analysis of thermal effect in aluminum alloy by repetition frequency pulsed laser,” Optik (Stuttg)., vol. 127, no. 20, pp. 10115–10121, Oct. 2016.

[23] P. Soltani and N. Akbareian, “Finite element simulation of laser generated ultrasound waves in aluminum plates,” Lat. Am. J. Solids Struct., vol. 11, no. 10, pp. 1761–1776, 2014.

[24] F. Augereau, D. Laux, L. Allais, M. Mottot, and C. Caes, “Ultrasonic measurement of anisotropy and temperature dependence of elastic parameters by a dry coupling method applied to a 6061-T6 alloy,” Ultrasonics, vol. 46, no. 1, pp. 34–41, 2007.

[25] B. Xu, Z. Shen, J. Wang, X. Ni, J. Guan, and J. Lu, “Thermoelastic finite element modeling of laser generation ultrasound,” J. Appl. Phys., vol. 99, no. 3, p. 33508, Feb. 2006.